

ADAPTIVE LOAD REDISTRIBUTION USING MINI-TEDS

A.D. Gardner* , J. Nitzsche** , J. Neumann** , K. Richter* , H. Rosemann* , R. Voss**
 *DLR Institute for Aerodynamics and Flow Technology, Bunsenstr. 10, 37073 Göttingen.
 **DLR Institute for Aeroelastics, Bunsenstr. 10, 37073 Göttingen.

Keywords: *mini-TED, fluid-structure coupling, DLR-TAU, HighPerFlex.*

Abstract

This article describes work in the DLR High Performance Flexible Aircraft (HighPerFlex) project to investigate mini trailing edge devices for adaptive load redistribution. The EU project AWIATOR showed the potential of mini-TEDs, but the increased rear wing loading and resulting nose-down pitching moment require further investigation. 2-D computations were carried out to investigate effective split-flap deployment angles. The calculations show that the optimal height of a mini-TED on an unknown profile in transonic flow cannot be predicted by scaling with the boundary layer thickness on the pressure-side trailing edge. The scope of the future work on structure-coupled 3-D computations on a trimmed aircraft is described.

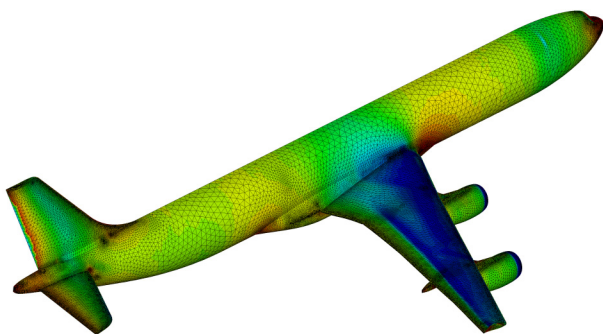


Fig. 1 HighPerFlex A340-300 half-configuration. The CENTAUR surface grid and contours of surface pressure coefficient are shown for the clean aircraft configuration.

Notation

Variables

C_D, C_d	Coefficient of drag
C_L, C_l	Coefficient of lift
α, Alpha	Angle of attack (degrees)
δ	Mini-TED deployment angle
ϕ	Wing sweep angle
y^+	Normalised grid first cell spacing
Ma	Mach number
Re	Reynolds number

Subscripts

$L_{0.5}$	Variable is measured at the local wing half-chord position
max	The maximum value of that variable
$2.5-D$	Refers to 2-D data transformed to 3-D for a simple wing at constant sweep, zero taper and zero twist

1 Introduction

The redistribution of load over a transonic wing can be achieved by relatively minor modifications to the wing shape using mini trailing edge devices (mini-TEDs). These were small split-flaps on the trailing lower edge of the wing or flaps, which can be deflected only in a downward direction. They are intended to act as a divergent trailing edge for cruise flight, and as Gurney flaps for low speed applications. A split-flap was selected as being more effective than a Gurney flap based on an experimental investigation of a supercritical Airbus profile [1].

This type of mini-TED was studied in the DLR-Airbus project AWIATOR [2] for their ability to increase the maximum lift and to decrease the drag of an A340-300 during cruise flight. The potential of the mini-TEDs to allow load redistribution on a wing was noted, potentially allowing an aircraft to spend a greater proportion of its flying time at close to design conditions. Load redistribution devices also theoretically permit load control under gust-buffeting and the reduction of maximum wing root bending moment. Mini-TEDs cause both bending and torsion of the wing, and a nose-down pitching moment, and so fluid-structure coupled (aeroelastic) computations on a trimmed aircraft are required to compute the true effect of the load redistribution.

The computations presented in this paper, undertaken under the project HighPerFlex, use an A340-300 half-configuration which includes the wing, fuselage, engine pylons and engine nacelles imported from the project AWIATOR. A tail assembly was added to this model (Fig. 1). The aircraft is to be trimmed computationally by varying the angle of the horizontal tailplane to minimise the pitching moment.

2 CFD tools

Computations presented in this article were performed with the DLR-TAU code [3]. A finite-volume solver was used on a hybrid unstructured grid consisting of 30 (2-D) or 22 (3-D) prismatic layers close to the surfaces and a tetrahedral or triangular field (Fig 2), generated using the CENTAURTM[4] unstructured grid generator. The prismatic layers were adapted during the computation to a target $y^+=1$ by movement of the wall-tangent cell boundaries, and the tetrahedral field was adapted to resolve fine structures by subdivision of the tetrahedra. A farfield radius of 50 aircraft lengths was used for the 3-D grids, and of 50 chord lengths for the 2-D computations. Use of the farfield vortex correction [5] was necessary for the 2-D computations to be independent of the farfield. The solver was run until a change of less than one drag count over 100 time steps was observed and then the grid

was adapted and the solver rerun. Grid convergence was defined as a change of less than one drag count between two adaptation steps, resulting in grids of around 160000 nodes in 2-D and 10 million nodes in 3-D. Unconverged points in the 2-D computations near maximum lift are included, but do not affect the angles of attack of interest in this study.

All computations were fully turbulent, using the Spalart-Allmaras turbulence model [6] with the Edwards modification (SAE) [7]. A central scheme was used with the method of Van-Leer [8] as the first order solver and AUSM-DV [9] as the second order solver. Gradient reconstruction was by Green-Gauss using the MUSCL scheme [10] for values at the cell boundaries.

The TAU deformation tool is used to adjust a volume grid based on a surface deformation. The movement of the surface points is transferred as a stiff movement to the layer of cells closest to the wall. An iterative wavefront method is then used to smooth the deformation into the main grid, such that the effect is localised. Large deformations can result in the movement of nodes such that bad cells are created. The maximum deformation of a structural part such that the resulting grid is valid is a function of the size of the surface cells (and thus of the Reynolds number), and of the grid quality, particularly the maximum tetrahedral sliver value. Grids from AWIATOR were not suitable for use in this project because the maximum tetrahedral sliver value of 250 caused the creation of bad cells at the required wingtip deformations. Careful CAD cleaning and deactivating cell-chopping in CENTAURTM reduced the maximum sliver below 20, allowing wingtip deformations of half the wingspan for a Navier-Stokes grid for flight Reynolds numbers. The resulting grid was 20% larger than that used in AWIATOR.

3 2-D computations

3.1 Geometry and conditions

The A340 wing has a varying profile and local chord length, so in the study of the wing, it

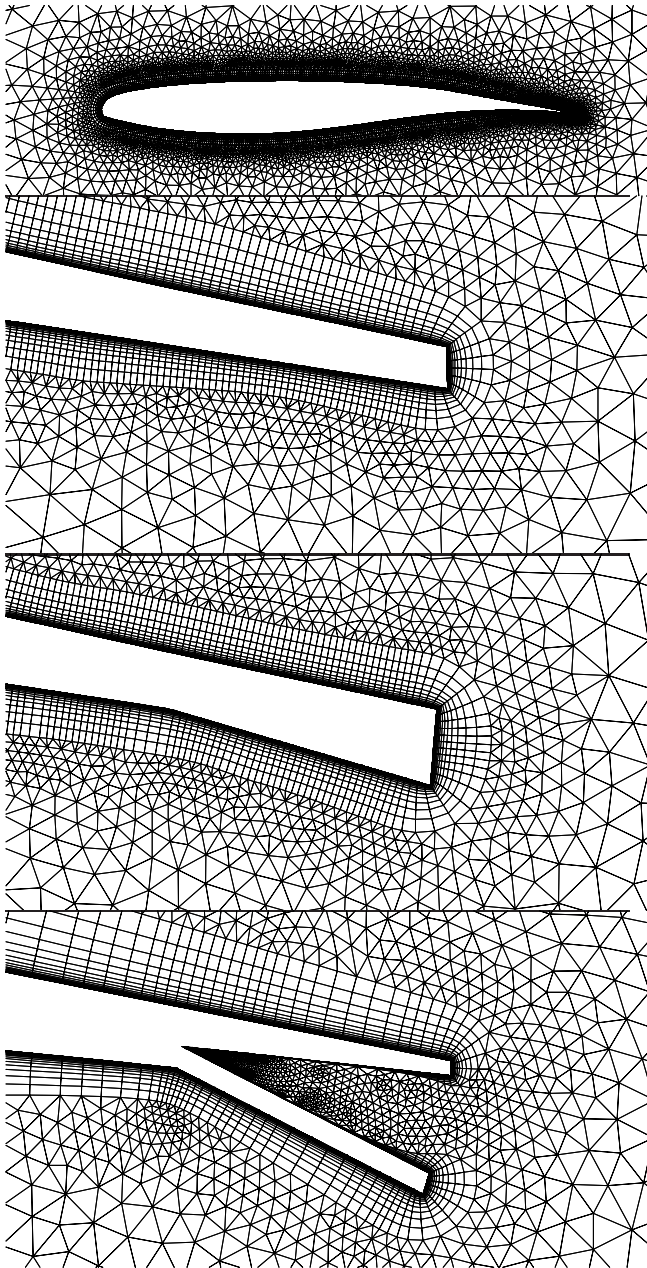


Fig. 2 2-D hybrid grids before adaptation showing the addition of a 7.5-degree wedge, to model a split-flap. A 2-D grid for a 20-degree open split-flap is shown at bottom, with cell-chopping and reduction of the structured layer height in the gap.

was divided into three parts; inboard of the first kink in the wing trailing-edge, outboard of the outer engine, and midboard, which contained the wing between these sections. Three slices were taken on curved sections, the geometry of which is defined by linearly varying the local sweep

angle between the leading and trailing edges of the wing. Fig. 3 has these cuts shown at their angle of attack in the 3-D aircraft, showing the change in profile, and the wing twist over the wing. Mach and Reynolds numbers were transformed with the half-chord sweep angle ($\phi_{L_{0.5}}$) to get the two-dimensional conditions (Tab. 1).

Condition	$\phi_{L_{0.5}}$ (deg.)	Ma	Re (million/m)
3-D Cruise	-	0.82	5.53
Inboard	18.99	0.78	4.94
Midboard	25.72	0.74	4.49
Outboard	26.78	0.73	4.41

Table 1 Flow conditions for the computations.

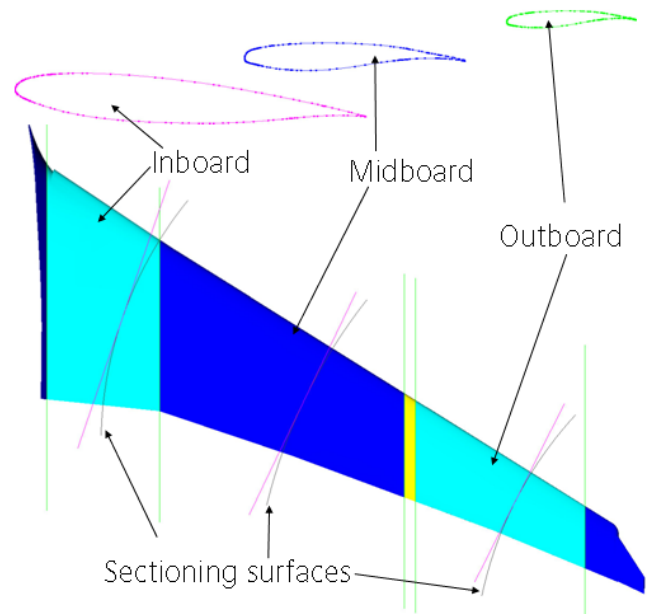


Fig. 3 Extraction of sections from the 3-D wing.

Results from AWIATOR suggested that a mini-TED should be designed as a split-flap of 2% chord [11]. Here the split-flaps were modelled as wedges of 2% chord, attached to the bottom of the profile (Fig. 2), which removed the need to model the gap between the split-flap. Tests showed that filling the gap made no difference to the quality of the simulation, but significantly reduced the number of nodes required,

due mainly to the flat pressure profile on the back edge of the wing being simply continued in the gap of the split-flap (Fig. 4). The speed-up in the computation was due as much to the improvement in stability and speed of convergence of the grids with the filled gap, as to the 20% reduction in total number of cells.

3.2 2-D polar results

2-D polars were calculated for each of the 2-D profiles from flow separation on the lower side to flow separation on the wing top for a range of mini-TED angles. The results for the midboard section are in Fig. 5. The mini-TED increases the lift at constant angle of attack (top right), and also increases the drag. The addition of a mini-TED also increases $C_{L_{max}}$, and decreases the drag at high lift coefficients (top left). The maximum glide-ratio (bottom left) is marginally improved ($\sim 1\%$). Of perhaps more interest is to note that an increase in local C_L by 0.3 can be attained by the movement of a mini-TED without risking separation on the wing. The pitching moment (Not shown in Fig. 5) changes linearly with the mini-TED angle at constant C_L .

The 2-D polars for the outboard section (Fig. 6) illustrate how the effects of the mini-TEDs are profile dependant. Notable here is that any addition of mini-TED angle to the base profile results in a poorer glide-ratio. As for the midboard section, an increase in the local C_L by 0.3 can also be attained by the movement of a mini-TED without risking separation on the wing. The comparison of these results shows that Giguere *et al*'s finding "...that the height of the Gurney scales with the boundary layer thickness" [12], is not generally applicable to finding the optimal height of split-flaps at transonic Mach numbers, since the effectiveness of the TED is much more strongly affected by the profile shape than by the trailing edge Reynolds number (Tab. 2). This supports the experimental findings of Richter and Rosemann on a similar profile in transonic flow [1]. However, all cases investigated confirmed Giguere *et al*'s guideline that effective mini-TEDs should be buried in the boundary layer.

The results from the inboard section are quite different from the other two sections (Fig. 7). An improvement in glide-ratio of $\sim 12.5\%$ is achievable, although the minimum drag for those polars increases enormously. Perhaps more interesting is that for this profile shape, the best glide ratio is achieved for a mini-TED of $\sim 43\%$ of the boundary layer height. Local C_L could again be increased by 0.3 without risking separation on the wing.

δ	Inboard	Midboard	Outboard
0.0	0.00	0.00	(0.00)
2.5	0.05	0.06	0.06
5.0	0.11	(0.13)	0.11
7.5	0.16	0.19	0.17
10.0	0.22	0.26	0.22
12.5	0.27	0.32	0.27
15.0	0.33	0.38	0.33
17.5	0.38	-	-
20.0	(0.43)	-	-
22.5	0.48	-	-
30.0	0.63	-	-
37.5	0.76	-	-

Table 2 Mini-TED height normalised with boundary layer height at the pressure side trailing edge. Optimal heights are in brackets.

4 Initial 3-D computations

Initial 3-D aerodynamic computations were undertaken to provide a baseline for the aeroelastic computations, and for the comparison with two dimensional computations. Mini-TEDs of 2% chord length were added at angles suggested by the 2-D computations by the addition of wedges to the trailing lower edge of the wing. The absolute width of the mini-TEDs varied with their position on the wing. They were created by the rotation of the lower wing trailing edge about the 98% chord line and filling the resulting gap. The relevant panels were swapped in CENTAURTM and the grid was regenerated with the settings of the clean configuration. This resulted in a grid with approximately the same

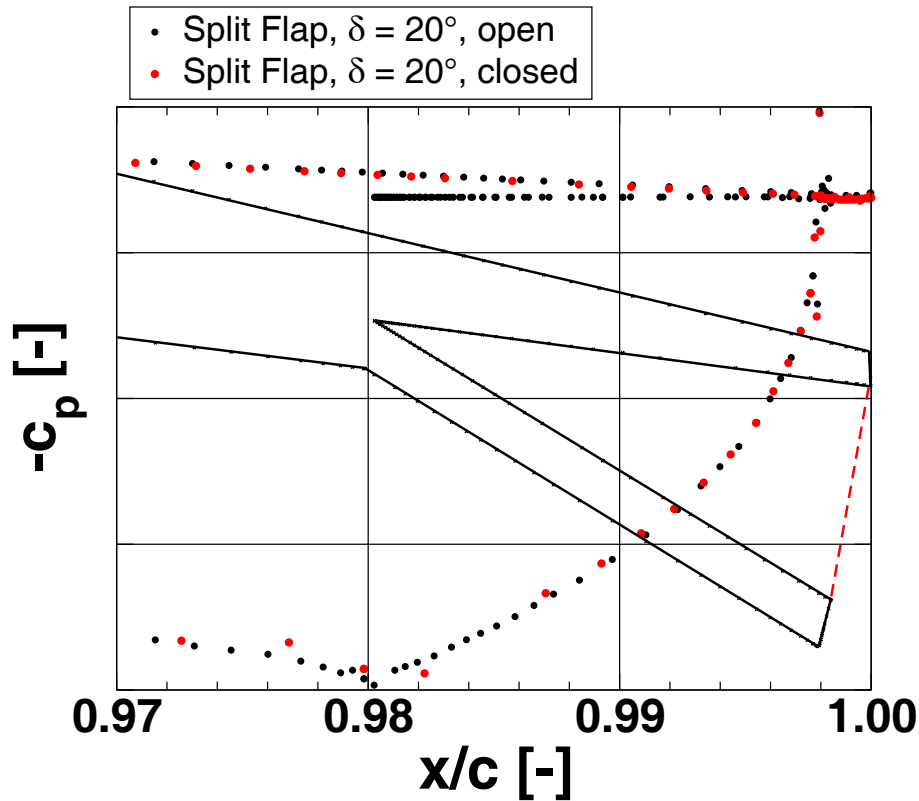


Fig. 4 Comparison of split-flap simulations with filled and open trailing edges. A340 2-D wing section WX9530, sweep transformed, fully turbulent. $Ma_{2D}=0.778$, $Re_{2D}=48 \times 10^6$, $\alpha=-0.45^\circ$.

number of cells for all configurations, with faster generation and better grid quality than a multi-block grid created with CENTAURTM. All 3-D computations presented here were performed for $C_L=0.52$ and a flight Reynolds number of 40 million based on the wing mean chord.

4.1 Comparison of 2-D and 3-D solutions

The pressure distributions from the 2-D clean computations were compared with pressure distributions from 3-D computations (Fig. 8) for the clean-case to assess the applicability of the 2-D computations to the 3-D case. The cut-planes for the 3-D configuration were in the flow direction, intersecting the respective 2-D profile cuts at half the local chord ($L_{0.5}$). The C_P values obtained from the 2-D polars were transformed back to 2.5-D, by using the local $\phi_{L_{0.5}}$ (Tab. 1). Points on the 2-D polars were selected such that their $C_{L_{2.5-D}}$ matched the local C_L for each of the 3-D

pressure distributions (Tab. 3).

Case	Inboard	Midboard	Outboard
3-D Cruise	0.456	0.568	0.602
2.5-D	0.435	0.568, 0.638	0.592

Table 3 Lift coefficients from 2-D and 3-D computations for Fig. 8.

As can be seen in Fig. 8, none of the pressure distributions are in excellent agreement between 2-D and 3-D. The inboard sections have qualitative agreement on the lower side of the profile, but the strong shock present in the 2-D computation is not present in the 3-D computation. It is notable that the $\phi_{L_{0.5}}$ used for this section is much lower than for the other configurations, due to the low angle of the wing trailing edge in the inboard section. Such a strong shock is an indication that the mean inclination of the flow to the profile is

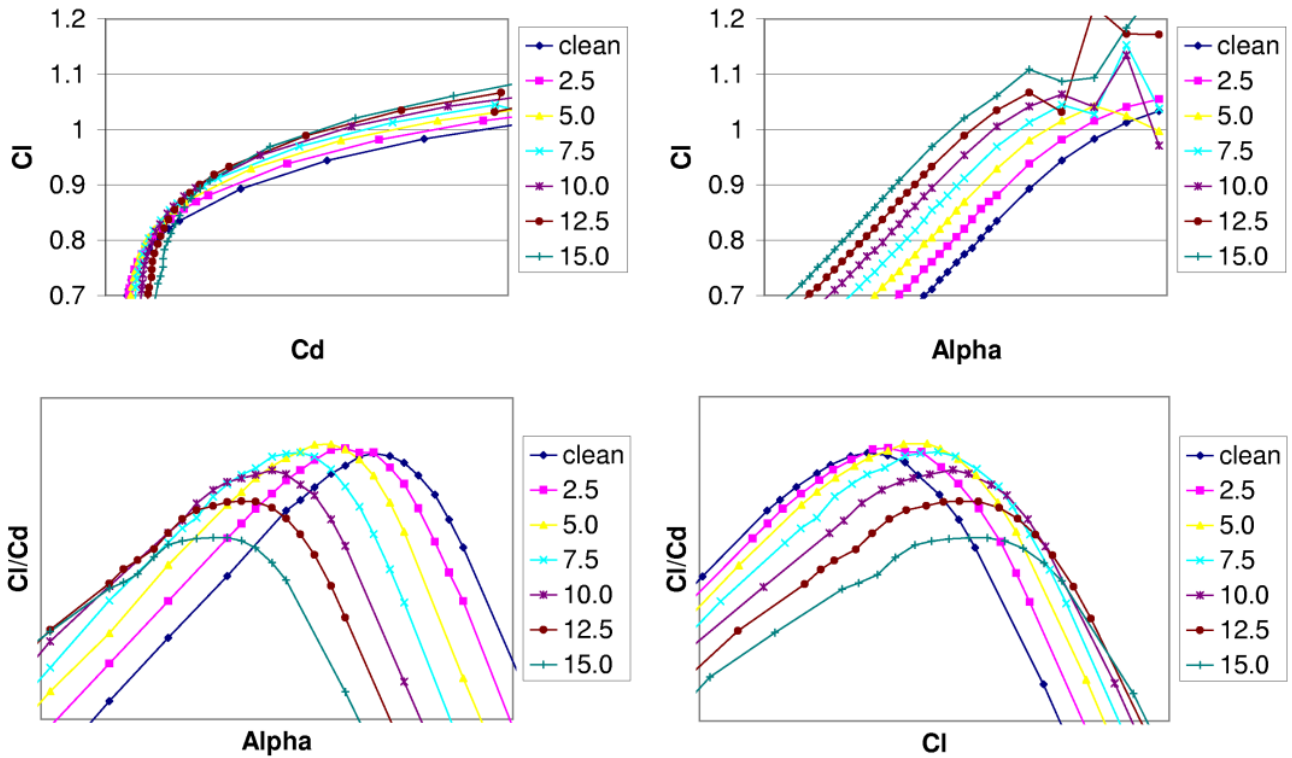


Fig. 5 2-D polars showing the change in coefficients for the midboard section. Legend shows the mini-TED deployment angle (δ) in degrees.

different than expected, indicating strongly three-dimensional flow.

The data from the midboard section is also not similar to the 3-D values. Here the effect of the engine nacelle on the wing makes the matching of the condition by C_L problematic, since the effect of the nacelle is to reduce the pressure on the bottom side of the wing. When a point on the 2-D polar is selected such that the pressure plateau is matched (Cp Match), then the shock position and the trailing edge pressures are also matched. In this case, however, the pressure on the lower side of the wing remains qualitatively similar to that from the 2-D computation, showing that the nacelle is significantly affecting flow in this region. The data from the outboard region matches well, except in the location of the shock. It is unclear why the shock location should have this difference, except from a wing-tip effect. The 3-D cut is taken about one local chord from the end of the wing (not including winglet).

Qualitative similarity was achieved between

the 2-D and 3-D computations for the midboard and outboard sections, which suggests that the 2-D computation will be useful as a guideline for the setting of the 3-D mini-TED angles. In the inboard section the strong 3-D effects of the flow must be taken into account, meaning that strong reliance on the 2-D results may not be possible.

4.2 Mini-TED effects in 3-D

Baseline computations were undertaken to assess the effect of mini-TEDs on the 3-D geometry, so that the order of the tailplane trimming angle and the change in wing root bending moment could be assessed. These baseline computations for the rigid aircraft are to serve as starting solutions for the aeroelastic computations. Various mini-TED angles were tested with the tailplane set at the reference angle (Tab. 4), and thus the results are for an untrimmed aircraft. A separate testing axis (not included here) involved testing the sensitivity of the aircraft to the tailplane trimming an-

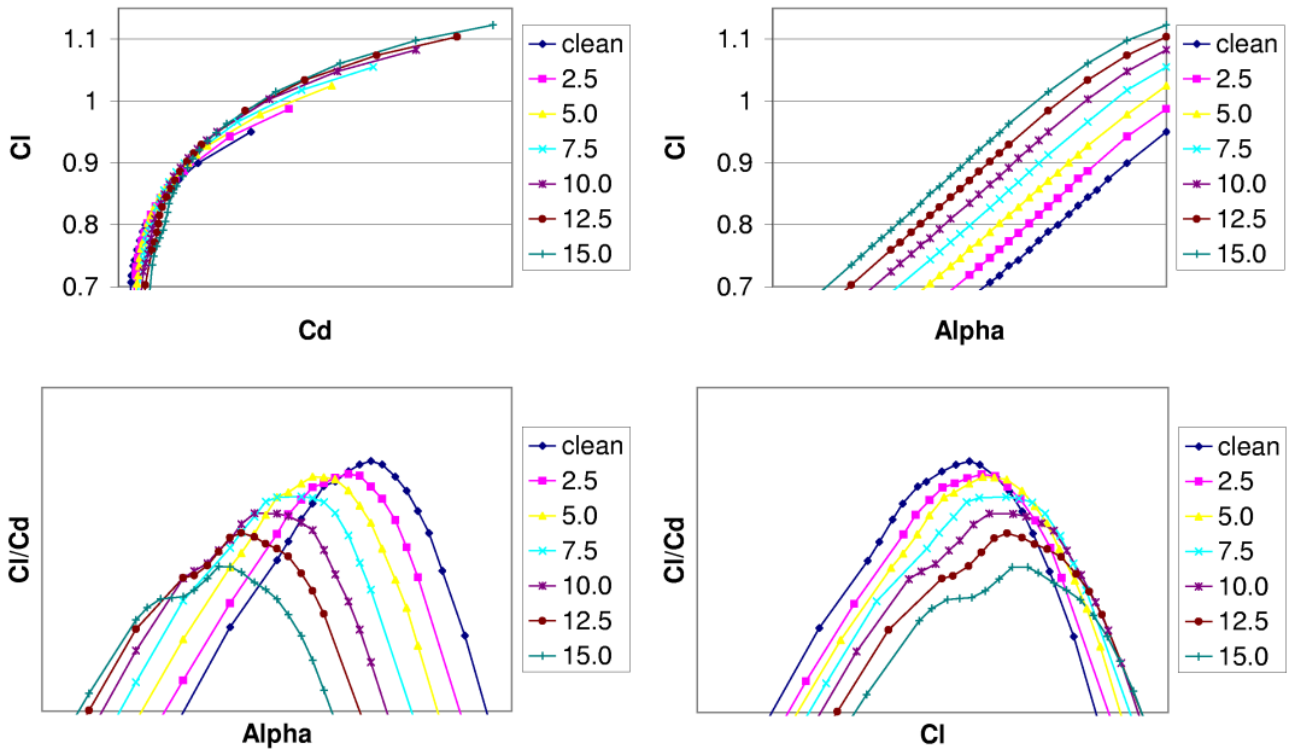


Fig. 6 2-D polars showing the change in coefficients for the outboard section. Legend shows the mini-TED deployment angle (δ) in degrees.

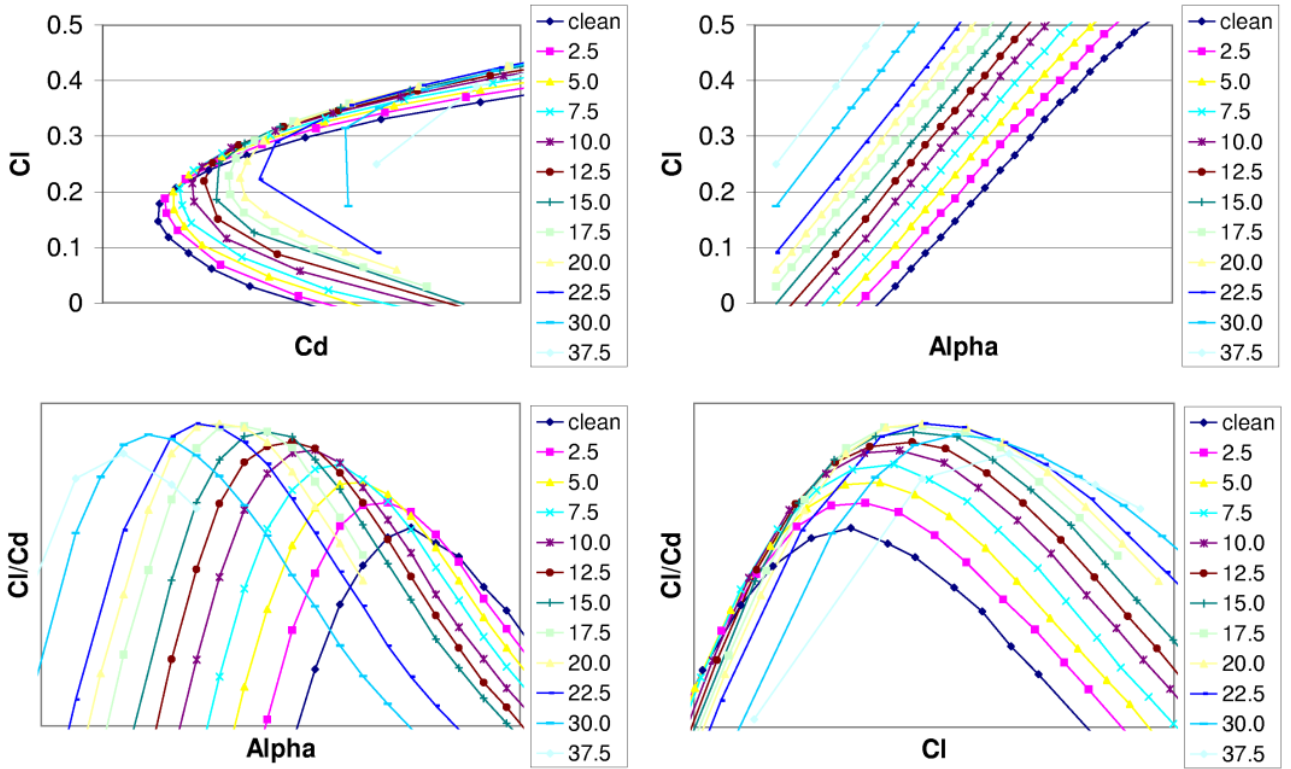


Fig. 7 2-D polars showing the change in coefficients for the inboard section. Legend shows the mini-TED deployment angle (δ) in degrees.

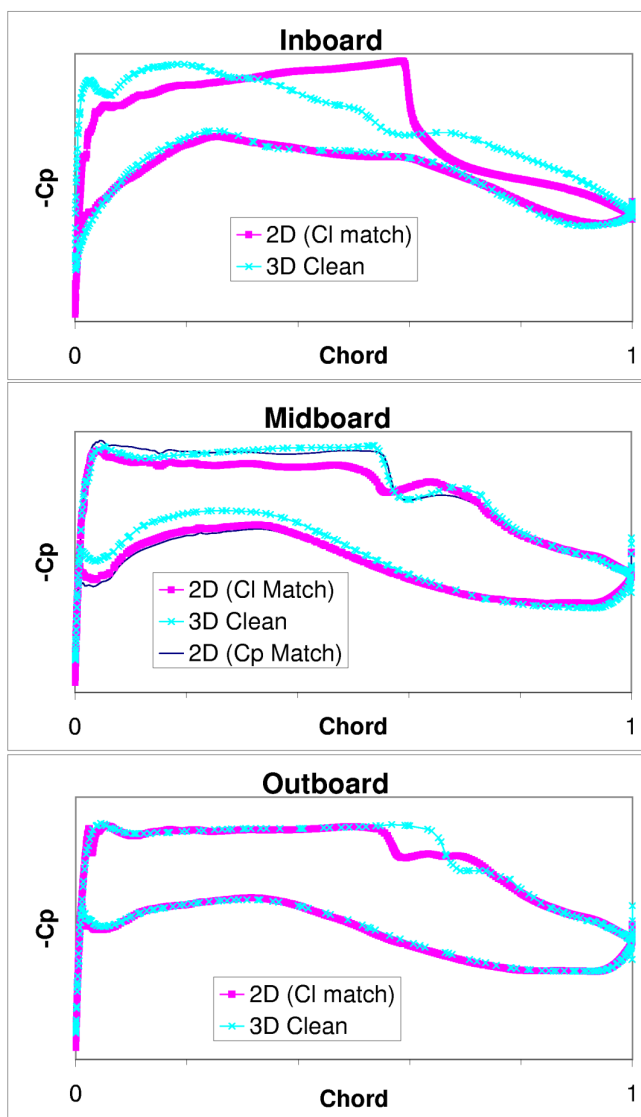


Fig. 8 Comparison of 2-D and 3-D pressure distributions. 2-D data is transformed to 2.5-D.

gle. All computations automatically set the aircraft pitch to achieve a lift coefficient $C_L=0.52$.

A reduction in the required aircraft pitch with respect to the clean case (21) to maintain the lift coefficient, and an increase in the drag is observed for all mini-TED configurations (Fig. 9). A simple analysis of the addition of mini-TEDS leads to the expectation that the movement of loading to the rear of the wing will always result in a reduced pitching moment for the aircraft. This was always observable for the 2-D computations, however in the 3-D case, the change in aircraft pitch alone shifts the load on the wing (vis-

Case	Inboard TED δ	Midboard TED δ	Outboard TED δ
21	0	0	0
22	0	0	5
23	0	0	10
24	0	5	0
25	0	10	0
26	10	0	0
27	20	0	0
28	90	0	0
29	20	10	10

Table 4 Test cases for the effect of mini-TEDs on the 3-D configuration.

ible in the root bending moment), changing the pitching moment, so that the addition of a mini-TED may also result in an overall increase in the pitching moment. It remains to be seen what the effect of the coupling will add to this effect.

5 Future goals in HighPerFlex

Work is continuing on aeroelastic computations in HighPerFlex. The 2-D computations are used to reduce the search-space for the 3-D computations. Initial coupled computations have been performed, and have demonstrated recovery of the jig-shape, and propagation of the solution between the TAU and NASTRAN solvers following a scattered data interpolation method based on radial basis functions (RBF) [13, 14, 15]. The aerodynamic surface deformation into the aerodynamic grid is performed by the TAU deformation tool. Work is continuing on a tool to automatically trim the aircraft using deformation of the horizontal tail plane. In this way, the additional drag, lift and aircraft pitch changes due to the tailplane will be included in the assessment of the efficiency of the mini-TEDs. In a final step in the project, the use of ailerons and rudders for the load redistribution on the wing will be compared to that of the mini-TEDs using the techniques developed here.

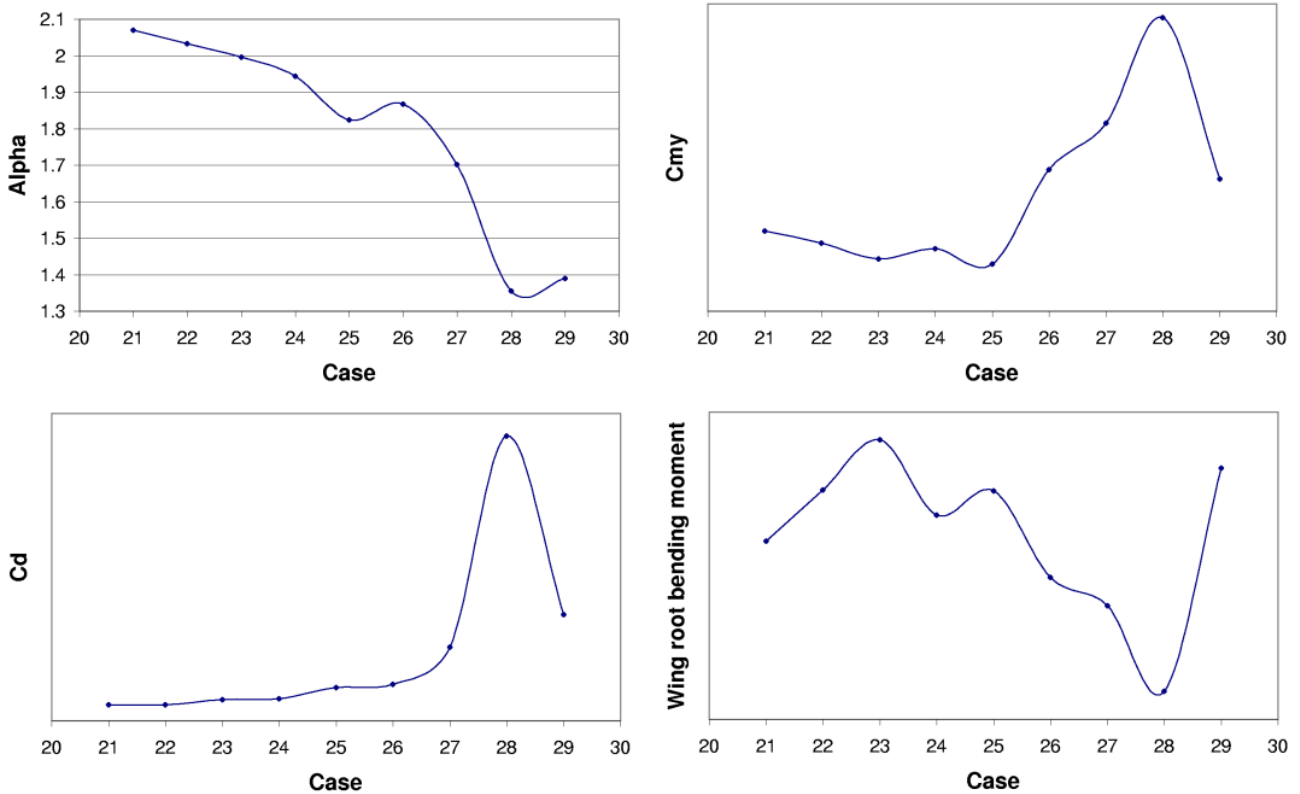


Fig. 9 Baseline computation results for mini-TEDs on the 3-D wing. Cases as Tab. 4.

6 Conclusion

The initial investigations into the use of mini-TEDs for load-redistribution on an A340-300 have been completed. The use of 2-D computations on wing slices has shown that mini-TED angles of under 10 degrees are likely to be most desirable, although the comparison with 3-D computations underlines the highly three-dimensional nature of the flow over the wing. Addition of mini-TEDs to the three dimensional geometry show that the reduction in aircraft pitch to maintain flight at constant lift coefficient leads to a change in wing loading. The consequent superposition of wing loadings due to the mini-TED and due to the change in pitch can provide changes in pitching moment which are in the opposite direction to those predicted by simple 2-D computations. Due to the unintuitive reaction of the 3-D geometry to changes, further computations with a trimmed aircraft and structure-coupling are expected to deliver particularly in-

teresting results. An appropriate structural model and aerodynamic grids for fluid-structure coupling have been developed, and the method of coupling has been demonstrated in principle. The aeroelastic computations will be performed once the tool for automatic aircraft trimming is finished.

References

- [1] Richter, K., Rosemann, H., *Experimental investigation of trailing-edge devices at transonic speeds*, The Aeronautical Journal of the Royal Aeronautical Society, pp185-193, 2002.
- [2] Hansen, H: *Application of Adaptive Trailing Edge Elements the AWIATOR Project*, CEAS/KATnet conference on Key Aerodynamic Technologies, Bremen, 20-22 June, 2005.
- [3] Gerhold, T., Friedrich, O., Evans, J. and Galle, M.: *Calculation of Complex Three-Dimensional Configurations Employing the DLR-TAU-Code* AIAA-paper 97-0167, 1997.

- [4] www.centaursoft.com
- [5] Thomas JL, Salas MD *Far-Field Boundary Conditions for Transonic Lifting Solutions to the Euler Equations*, AIAA Journal, V24, N7, pp1074-1080, 1986.
- [6] Spalart, P. R., Allmaras, S. R., *A one-equation turbulence model for aerodynamic flows*, AIAA Paper 92-0439, 1992.
- [7] Edwards, J.R., Chandra, S., *Comparison of Eddy Viscosity-Transport Turbulence Models for Three-Dimensional, Shock-Separated Flow-fields*, AIAA Journal, Vol. 34, No. 4, April 1996.
- [8] Van Leer, B., *Flux vector splitting for the Euler equations*, Proc. 8th International Conference on Numerical Methods in Fluid Dynamics, Springer-Verlag, Berlin, 1982.
- [9] Wada, Y., Liou, M.-S., *A flux splitting scheme with high resolution and robustness for discontinuities*, AIAA Paper 94-0083, 1994.
- [10] Van Leer, B., *Towards the ultimate conservative difference scheme. V. A second-order sequel to Godunov's method*, Journal of Computational Physics, V32 pp101-136, 1979.
- [11] Richter, K.: *Druckverteilungsmessung am 2D-Profil VC-Opt mit split Flaps im Transonischen Windkanal Göttingen*, Internal Report IB-224-2004-C-01, DLR, 2003.
- [12] Giguere, P., Lemay, J., Dumas, G.: *Gurney flap effects and scaling for low-speed airfoils*, AIAA paper 95-1881, 1995.
- [13] Heinrich, R., Ahrem, R., Günther, G., Kersken, H.-P., Krüger, W.-R., Neumann, J.: *Aeroelastic Computation Using the AMANDA Simulation Environment*, CEAS Conference on Multidisciplinary Aircraft Design and Optimization, Köln, 25.-26. June 2001.
- [14] Neumann, J., Einarsson, G.Ó., Schütte, A., *Multidisziplinäre Simulation eines rollenden, generischen Deltaflügels - Kopplung von Aerodynamik, Flugmechanik und Strukturmechanik*, DGLR Jahrbuch 2005, pp1297-1305, 2005.
- [15] Ahrem, R., Beckert, A., Wendland, H., *A new multivariate interpolation method for large-scale spatial coupling problems in aeroelasticity*, IFASD 2005.